PCCP

Accepted Manuscript

ROYAL SOCIETY OF CHEMISTRY

www.rsc.org/pccp

PCCP

ARTICLE

Parahydrogen Enhanced NMR Reveals Correlations in Selective Hydrogenation of Triple Bonds over Supported Pt Catalyst

Received 00th January 20xx,
Accepted 00th January 20xx

DOI: 10.1039/x0xx00000x

www.rsc.org/

Ronghui Zhou,[a] Wei Cheng,[b] Luke M. Neal,[b,†] Evan W. Zhao,[a] Kaylee Ludden,[a] Helena E. Hagelin-Weaver[b,*] and Clifford R. Bowers[a,*]

Parahydrogen induced polarization using heterogeneous catalysis can produce impurity-free hyperpolarized gases and liquids, but the comparatively low signal enhancements and limited scope of substrates that can be polarized pose significant challenges to this approach. This study explores the surface processes affecting the disposition of the bilinear spin order derived from parahydrogen in the hydrogenation of propyne over TiO_2-supported Pt nanoparticles. The hyperpolarized adducts formed at low magnetic field are adiabatically transported to high field for analysis by proton NMR spectroscopy at 400 MHz. For the first time, the stereoselectivity of pairwise addition to propyne is measured as a function of reaction conditions. The anticorrelation between partial reduction selectivity and stereoselectivity of pairwise addition is revealed. The systematic trends are rationalized in terms of a hybrid mechanism incorporating non-traditional concerted addition steps and well-established reversible step-wise addition involving the formation of a surface bound 2-propyl intermediate.

Introduction

Parahydrogen-induced polarization (or PHIP)[1-7] is a robust, inexpensive and scalable method for continuous production of nuclear spin hyperpolarized gases and liquids for enhanced sensitivity NMR spectroscopy and imaging. The nuclear spin symmetrization order inherent to parahydrogen is transformed into NMR-observable hyperpolarization by symmetry breaking chemistry. High-field NMR signal enhancements of three to four orders of magnitude are possible,[2, 6] but only if H_2 adds to the substrate in a pairwise fashion (*i.e.* both protons originate from the same H_2 molecule).

Recent innovations have extended the applicability of PHIP.[7-16] Oxide-supported metals, pure oxide catalysts or dispersed single-atom catalysts can deliver impurity-free hyperpolarized gases and liquids.[10, 11, 17-23] Parahydrogen enhanced NMR also provides a unique tool for mechanistic studies of hydrogenation catalysis[3, 5, 24-28] due to its sensitivity to concerted addition.[29] Pairwise addition to triple and double bonds over metals like Pd and Pt dispersed on various oxides like TiO_2, Al_2O_3, ZrO_2, and SiO_2 have been studied using the high-field PASADENA-PHIP technique, where partial reduction selectivity and pairwise addition selectivity are independently measurable.[30] In the present work, we focus on propyne hydrogenation over Pt/TiO_2 catalysts in a continuous-flow hydrogenation reactor setup. Correlations between stereoselectivity and partial reduction selectivity (propene vs. propane) of pairwise addition are examined by parahydrogen enhanced NMR for the first time, revealing the roles of the 2-propyl intermediate.

The decades-old Horiuti-Polanyi mechanism for hydrogenation of alkenes over metals is still generally accepted as the predominant path for hydrogenation of alkenes over metals like Pt and Ir.[31] The central feature of this mechanism is step-wise addition involving a surface-bound alkyl intermediate (e.g. 2-propyl, for propene hydrogenation). However, the preservation of the proton spin-correlation leading to the observation of PHIP signals requires a pair-wise addition process that is not favored by a step-wise path due to rapid H atom diffusion on the metal surface. The existence of a minor direct saturation route on Pt was identified in the early work of Bond,[32, 33] and addition of molecular H_2 has been reported for relatively inert metals like Ag and Au.[34, 35] Our working hypothesis is that the 2-propyl species of the traditional mechanism plays a central role in the interconversion of the *cis* and *trans* dispositions of parahydrogen bilinear spin order on propene. In our model, *cis-trans* isomerization competes with desorption of propene and second reduction to propane.

Parahydrogen enhanced NMR is uniquely sensitive to the stereoselectivity of pairwise addition of H_2 to propyne. The statistical distribution of an isotopic label (e.g. deuterium) does not directly probe pairwise addition and also introduces kinetic isotope effects. We explore the relationship between pairwise partial reduction selectivity (i.e. selectivity to propene versus propane) and pairwise addition stereoselectivity (*anti*- versus *syn*-addition). Systematic trends in the experimental data are interpreted in terms of well-established surface processes and species associated with hydrogenation over Pt. The *cis/trans* disposition of the singlet spin order on propene will be

[a] Department of Chemistry, University of Florida, Gainesville, FL USA 32611.
[b] Department of Chemical Engineering, University of Florida, Gainesville, FL USA 32611.
†Department of Chemical & Biomolecular Engineering, North Carolina State University, Raleigh, NC 27695.
Electronic Supplementary Information (ESI) available. See DOI: 10.1039/x0xx00000x

randomized by fast methyl rotation upon formation of the 2-propyl intermediate.

Experimental Section

Catalyst Preparation. The reaction studies reported here were performed over a TiO_2 supported Pt nanoparticle catalyst (nominal Pt loading of 1% by weight) prepared by the deposition-precipitation method.[14] The $H_2PtCl_6{\cdot}6H_2O$ precursor (0.053 g, Alfa Aesar, CAT # 036259) was dissolved in 5 mL deionized H_2O and added to an aqueous suspension of the TiO_2 support (1.981 g support, Alfa Aesar, CAT #44429, in 100 mL deionized H_2O). Platinum hydroxide was deposited onto the support by increasing the pH of the suspension to 11 with a dilute NaOH (2.5 mM) solution, followed by neutralization by an acetic acid solution (pH = 7, after stirring overnight). The mixture was then filtered, re-dispersed in deionized water, and filtered a second time after stirring overnight. The pre-catalyst was dried at 105 °C overnight, before being heat treated in air at 350 °C for three hours.

Catalyst Characterization. The actual metal loading of the prepared catalyst was determined by inductively coupled plasma-atomic emission spectroscopy (ICP-AES) on a Perkin-Elmer Optima 3200 RL. The Pt/TiO_2 catalyst material was fused with sodium peroxide at 500 °C for 1 hour followed by dissolution in water and neutralization with hydrochloric acid. From the measured concentration of metal species in the fusion solution, the actual Pt loading was determined to be 0.7 wt% on the TiO_2 support. The active Pt metal surface area was measured by CO chemisorption on a ChemBET 3000™ (Quantachrome Instruments, Inc.) after reduction in 5% H_2 in nitrogen at 170 °C for 30 min. A CO uptake of 730 μL/g was measured, and using this CO uptake an average particle size of 1.1 nm and a 90% dispersion was calculated (see *ESI* for details).

Scanning TEM (STEM) images were collected on a probe aberration corrected JEOL JEM-ARM200cF instrument with a cold-field emission electron gun. See *ESI* for details. Representative STEM images of the catalyst are shown in Figures 1(a) and (b). The presence of Pt on the TiO_2 support was confirmed by energy-dispersive X-ray spectroscopy (not shown).[36] A histogram of the Pt particle diameters, shown in Figure 1(c), was constructed by analysis of the STEM images using the ImageJ[37] image analysis software. Single Pt atoms were not included in the distribution as they may easily fuse with large particles under reaction conditions. Based on the statistics of 200 particles, the average Pt particle size is found to be 1.1 nm with a standard deviation of 0.2 nm, in agreement with the size estimation obtained by CO chemisorption.

Hydrogenation Reactor. Our hydrogenation reactor consists of a 0.25 in. o.d. U-shaped glass tube mounted inside a ceramic heating element where the temperature of the catalyst bed can be varied from ≈ 25 °C to 400 °C. The reactor was mounted just above the bore opening of a 9.4 T Bruker Ultrashield™ actively shielded magnet where the fringe field is 5 mT. The reaction temperature is monitored using a K-type thermocouple probe inserted directly into the catalyst bed. A continuous stream of 50% para-enriched H_2 gas (p-H_2) was generated by passing normal hydrogen (n-H_2) through a 0.25 in. copper coil filled with activated charcoal and immersed in a liquid N_2 (77 K) filled dewar. The parahydrogen fraction was confirmed by NMR. Reactant gas mixtures with varying composition containing H_2 (normal or para-enriched), propene, and N_2 were prepared by controlling the flow-rate of each gas using three separate mass flow controllers (Alicat Scientific, Inc.). The outlets of the mass flow controllers were combined at 1 bar pressure with a Swagelok cross. The gas mixture was delivered at a total flow rate of 400 mL/min to the reactor inlet using PFA tubing (0.0625 in. i.d., 0.125 in. o.d.). PFA tubing connected to the outlet of the reactor U-tube passes through a Swagelok reducing union connected to the top of a 1 m long larger diameter (0.25 in. o.d.) stainless steel tube that extends down to the probe and is attached at the bottom to the threaded 10mm o.d. NMR tube using a Swagelok compression fitting with a Teflon adapter. The gas is transported to the bottom of the NMR tube through a thin glass capillary inserted into the terminus of the PFA tubing.

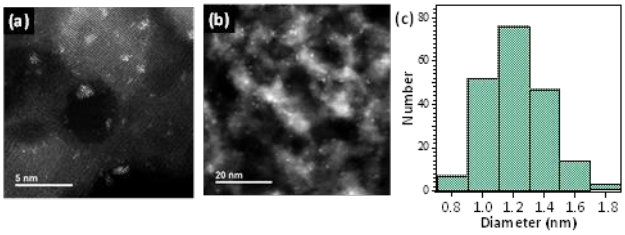

Figure 1. (a,b) Transmission electron micrographs of the Pt/TiO_2 catalyst at two different magnifications. (c) Histogram of Pt particles sizes based on 200 particles.

Prior to reactions, catalysts were reduced in pure H_2 at 170 °C for 30 minutes at a flow rate of 200 mL/min followed by an N_2 purge at the same flow rate for 30 min. At a reactant gas flow rate of 400 mL/min, the transport time from the reactor outlet to the NMR detection coil is 0.5 s.

NMR spectra were acquired with a Bruker Avance 400 MHz (B_0 = 9.4 Tesla) NMR spectrometer fitted with a standard Bruker 10 mm liquids probe. A total of 16 NMR signal transients were averaged using an 8-step phase cycle and a 20 μs 90° pulse. Spectra were acquired on the continuously flowing reactor effluent stream using a recycle delay of 2 s. The hyperpolarized or thermally polarized NMR signals of propene and propane were corrected for relaxation losses, as described in *the ESI*.

Theory

Figure 2 presents a simplified scheme for the hydrogenation of propyne that incorporates hydrogenation of propene to propane by the Horiuti-Polanyi (HP) mechanism.[32] The transformations involving bilinear spin order introduced with p-H_2 are emphasized by coloring the H atoms originating as p-H_2 in red. Surface adsorbed H_2 molecules and H atoms in random nuclear spin states are colored in blue. Pairwise addition of H_2 to propyne can occur by either *syn* or *anti* addition, resulting in the *cis* or *trans* dispositions of the bilinear spin order on propene. Desorption of propene competes with further reduction to propane and half-hydrogenation to the 2-propyl

species, as was observed by Somorjai et al.[38] using infrared-visible sum frequency generation vibrational spectroscopy.

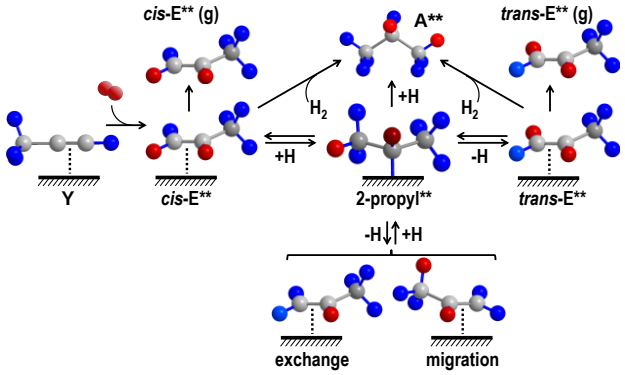

Figure 2. Simplified scheme showing the surface processes associated with hydrogenation of propyne to propene and propane on a Pt surface. Y=propyne, E=propene, A=propane. ** denotes bilinear scalar order. Atom color coding: grey=carbon; blue=hydrogen in random proton spin state; red=hydrogen originating as singlet-state H_2. For clarity, adsorption and dissociation of hydrogen have been omitted, and bonding of H atoms and H_2 molecules to the surface is not shown. The 2-propyl species mediates various surface processes: step-wise **addition**, leading to propane; double bond **migration**; methyl rotation, resulting in *cis-trans* isomerization; H atom exchange, resulting in loss of spin correlation.

According to the Horiuti-Polanyi mechanism for propene hydrogenation,[31, 32, 39, 40] 2-propyl can revert to π-bonded propene or it may incorporate a second H atom to yield free propane. Iteration of this reversible step accounts for the pattern of deuteration in the alkane when D_2 is used.[33, 39, 41, 42] A "direct saturation" route involving concerted addition of surface-adsorbed molecular H_2 to the alkene was noted by Bond and its existence as a minor pathway for supported metals like Pt is consistent with the observation of a PHIP effect with low pairwise selectivity of a few percent as we reported previously.[14] The bonding of H_2 to the metal surface may be analogous to that found in certain transition metal complexes.[28, 43] On some metals such as the Au-based systems, evidence suggests that a direct saturation path involving surface-adsorbed H_2 may dominate.[34]

The 2-propyl species mediates various processes that may be distinguished by their effect on the disposition of the two-spin scalar order: rotation, manifested as a loss of stereoselectivity; exchange, resulting in a loss of spin order; double bond migration, resulting in intensity changes in the propene CH_3 and CH_2 signals; and addition of a second hydrogen, producing propane. The combination of PHIP and thermally polarized NMR allows us to probe individual steps in the hydrogenation mechanism. Intense PHIP NMR signals on propene can also result from the dehydrogenation of propene to propyne followed by pairwise re-hydrogenation back to propene.[14]

The two variants of hydrogenative PHIP are referred to as PASADENA (parahydrogen and synthesis allow dramatically enhanced nuclear alignment), where hydrogenation reaction and NMR detection is carried out entirely at high magnetic field,[1, 2] and ALTADENA (adiabatic longitudinal transport after dissociation engenders net alignment).[4] In the ALTADENA effect, hydrogenation is performed at low magnetic field, where the strong coupling regime occurs, followed by "adiabatic" transport to high field for NMR detection. The two variants yield distinctly different NMR signal patterns. PASADENA produces antiphase multiplets and ALTADENA yields in-phase multiplets with net alignment. While most of the prior studies reported in the literature employed a PASADENA configuration where the hydrogenation catalyst is placed at the bottom of the NMR tube in a standard liquids NMR probe,[18, 44] ALTADENA offers significant advantages, as a conventional continuous-flow hydrogenation reactor design can be employed which allows more reliable control of the temperature in the catalyst bed (which is crucial in kinetic studies of exothermic reactions, which can have large temperature gradients)[45] since a thermocouple can be placed in direct physical contact with the catalyst. Furthermore, the in-phase ALTADENA net alignment multiplet signal patterns are more robust against destructive interference losses due to inhomogeneous magnetic fields or flowing conditions. In contrast, the antiphase multiplet patterns generated in the PASADENA effect are extremely sensitive to the line widths relative to the J-coupling. Destructive interference complicates the quantitative analysis of the signal amplitudes in PASADENA spectra.

A key difference between the PASADENA and ALTADENA variants concerns the disposition of bilinear spin order in the hydrogenation adduct. When adducts are formed at high field with weak coupling among chemically inequivalent sites, the bilinear spin order remains localized. Under PASADENA conditions, *syn* or *anti* addition to propyne yields signal intensity only on H^1 and H^3 or H^1 and H^2, respectively, using the numbering scheme defined in Figure 3. Hence, the stereoselectivity is in principle calculable from the relative peak area integrations, though in practice, accurate determination still requires line shape fitting to account for effects of destructive interference which are typically unavoidable. A different type of complication occurs in the ALTADENA mode: the scalar order originating as p-H_2 is distributed among all spins in the strong-coupling network. While such sharing may be desirable for some purposes, it complicates the analysis of the pairwise addition stereoselectivity. For instance, irrespective of the stereoselectivity of pairwise addition to propyne, propene ALTADENA signal enhancement is observed on both H^2 and H^3 peaks. Nevertheless, *syn* and *anti* addition yield distinctly different propene ALTADENA spectra, and the stereoselectivity can still be quantified by spectral fitting to density matrix simulations, *despite the complication of sharing of the parahydrogen spin order*.

Details of the density matrix spectral simulations are provided in the *ESI*. The 6 protons of propene are divided into four chemically inequivalent sets, labeled 1-4, with chemical shifts (in ppm) of 5.85, 5.03, 4.91, 1.72, respectively, and non-negligible J-couplings (in Hz) J_{12}=16.8, J_{13}=10, J_{14}=6.4, J_{23}=2.1. The geminal coupling in the methyl group is taken to be 15 Hz (though it is immaterial to the simulations). At 400 MHz, each of the sets of protons is weakly coupled with respect to all the others. Numerical density matrix calculations were performed to simulate both *syn* and *anti* addition of p-H_2 to propyne.

Additionally, we simulated the spectrum that results from addition across the triple bond followed by double bond migration. The dynamical model and simulation details are described in the *ESI*. The density operator is propagated numerically using SpinDynamica[46] running in Wolfram Mathematica™. This quantitative numerical approach automatically incorporates the spin dynamics near level anti-crossings that can potentially occur during the transport from low to high magnetic field.[47] Spin relaxation effects were not included in our SpinDynamica simulations.

The simulated ALTADENA spectra corresponding to *syn* and *anti* addition are shown in the lower two panels of Figure 3. The top panel presents an ALTADENA spectral simulation for pairwise addition (*syn* or *anti*) followed immediately by double bond migration. Note that in this simulated spectrum, the intensity at the H^2 and H^3 chemical shifts is significantly smaller than in the spectra for the *cis* or *trans* dispositions of the bilinear spin order in propene. Neglecting this contribution, an NMR spectrum $S(\nu)$ resulting from pairwise addition with arbitrary stereoselectivity is expressed as a linear combination of *syn* and *anti* addition spectra:

$$S(\nu) = c_{cis}S_{cis}(\nu) + c_{trans}S_{trans}(\nu) \quad (1)$$

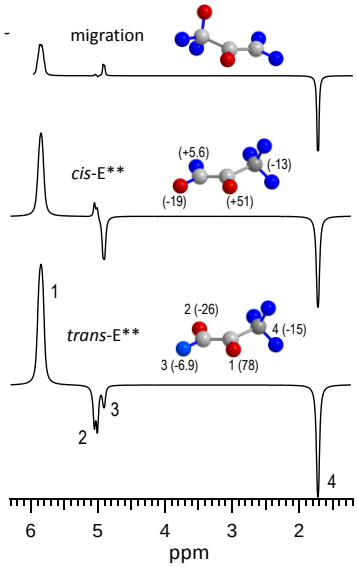

Figure 3. Density matrix simulations of the ATLADENA spectra of propene (E) formed with *cis* and *trans* dispositions of the bilinear spin order. Atoms coloured in red are those originating as p-H_2. Numbers in parenthesis represent the calculated percent Zeeman spin polarization on each proton following transport of the molecules to high field. The simulated spectrum resulting from double bond migration (via the 2-propyl intermediate) is shown in the top panel.

The percent *syn* addition stereoselectivity is defined as

$$\%\ syn\ \text{addition stereoselectivity} \equiv 100\,\% \times \frac{c_{cis}}{c_{cis} + c_{trans}} \quad (2)$$

The validity of our density matrix simulations and fitting procedure was evaluated by two independent methods.

Method 1: A series of ALTADENA spectra were acquired in which the flip angle θ of the NMR read pulse was varied from 45° to 90° in 15° steps while fixing all other acquisition parameters and reaction conditions. By changing the NMR pulse flip angle θ, the relative contributions of the in-phase and antiphase nuclear spin magnetizations created in the ALTADENA effect are varied.[4] As can be seen in Figure S2, substantial qualitative changes in the experimental line shapes of the propene CH_2 protons are seen across the series of spectra acquired at $\theta = 45$, 60, 75, and 90° at 350 °C. SpinDynamica spectral simulations for pairwise *syn* and *anti* addition to propyne were performed for the same set of θ used in collecting the experimental spectra. For each θ, the experimental spectrum was fit to a linear combination of simulated *syn* and *anti* addition spectra (eqn (1)), and the best-fit values of the weighting coefficients were then used to calculate the *syn* addition stereoselectivity by eqn (2). The fits, which are superimposed on the experimental spectra in Figure S2, consistently yield a *syn* addition stereoselectivity of 90 ±2 % across the series of different flip angles.

Method 2: the catalyst reactor bed was moved to a position just a few cm above the NMR probe within the bore of our 9.4 T superconducting NMR magnet. At this reaction field, which was measured to be 2.7 T, the density matrix spectral simulations (see Fig. S3, ESI) show that there is negligible polarization transfer to ancillary protons not belonging to one of the magnetically equivalent sets incorporating the protons originating as parahydrogen. The PASADENA mode spectrum shown in Fig. S4 was acquired using a 45° read pulse. The stereoselectivity was obtained from a least squares fit to a linear combination of spectra simulating *syn* and *anti* addition. At a reaction temperature of 250 °C, the stereoselectivity (see ESI) obtained in the PASADENA experiment run at 2.7 T is found to be the same as the value obtained for the ALTADENA experiment run with the same catalyst and same temperature but at a reaction field of 5 mT.

Results and Discussion

Temperature Dependence. Figure 4(a) presents the 400 MHz proton spectrum of the reactor efflux obtained in the steady-state using a 140/240/20 mL/min N_2/n-H_2/propyne reactant gas mixture (12:1 n-H_2:propyne, 400 mL/min total flow rate, 1 bar total pressure) at a reactor temperature of 350 °C. Under these reaction conditions, strong signals are obtained from both propene and propane (*vide infra*). Reactions with n-H_2 yield adducts with random spin states and spin polarization develops due to relaxation during transit into the high magnetic field of the NMR spectrometer. At a flow rate of 400 mL/min, we estimate that the proton spin polarization on propene and propane reaches 15-20% of its fully equilibrated value in our 9.4 T Bruker Ultrashield Magnet (see *ESI*). The large broad peak centred at ≈4.7 ppm is due to the o-H_2 component of the un-reacted n-H_2 gas. Superimposed on the left shoulder of this broad peak is the propene methine proton (H^1). Peaks at 4.91 and 5.03 ppm represent the methylene protons in the *cis* (H^3) and *trans* (H^2) positions relative to H^1. The CH_3 signals of

propene (H^4) and propyne, which are un-resolved in this spectrum, give rise to the peak at 1.7 ppm. The CH_2 and CH_3 multiplets of propane (H^5 and H^6, respectively) occur in the usual 1:3 intensity ratio. The signals in the spectrum recorded using n-H_2 are proportional to the total reduction (pairwise plus random) of propyne to propene and propane.

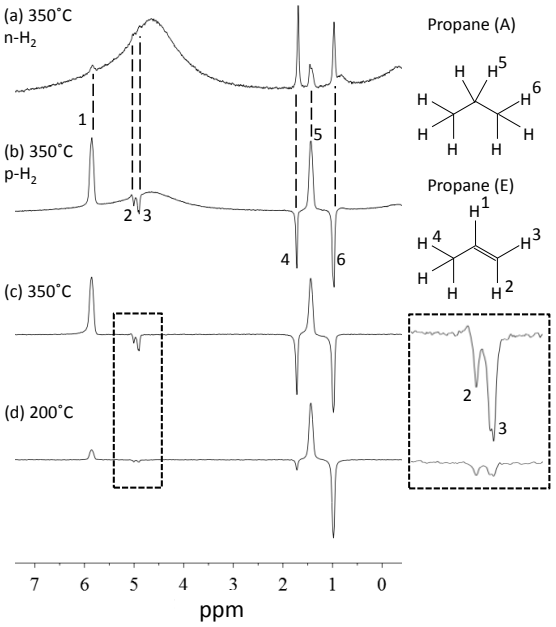

Figure 4. 400 MHz proton NMR spectra acquired on the effluent gas flowing out of the catalyst bed using a 140/240/20 mL/min $N_2/H_2/C_3H_4$ (12:1 H_2:propyne) reactant mixture. (a) Spectrum obtained using n-H_2 at a reactor temperature of 350 °C. (b) Same mixture and temperature but using p-H_2. (c) Difference spectrum obtained by subtraction of the spectrum acquired with n-H_2 from the one obtained with p-H_2 followed by baseline correction. (d) Difference spectrum at 200 °C. The dashed box present expansions around the propene CH_2 region. Peaks labeled 5 and 6 represent CH_2 and CH_3 on propane, respectively. All four spectra are plotted using the same vertical scaling.

When the experiment was run with p-H_2 under otherwise identical conditions, the spectrum shown in Figure 4(b) was obtained. The intensity of the broad o-H_2 peak of the unreacted 50% para-enriched gas is lower in the spectrum acquired using para-enriched gas. Both propene and propane exhibit intense ALTADENA multiplet patterns. The observed spectrum is actually a superposition of ATLADENA signals and much weaker thermally polarized signals resulting from random addition. The pure ALTADENA spectrum shown in Figure 4(c) was obtained by subtracting the spectrum acquired with n-H_2 from the one acquired with p-H_2. The residual o-H_2 peak resulting from the differing o-H_2 contents used in the two experiments has been removed by cubic spline interpolation.

Consistent with the theoretical prediction, the CH_2 and CH_3 signals exhibit a 1:-1 intensity ratio, where the spin-state population differences across all transitions involving the methyl protons are inverted with respect to the conventional Boltzmann distribution (the normal integral ratio is 1:3). The propene methyl protons (H^4) exhibit a strong emission phase signal. This multiplet signal enhancement, which derives from the distribution of scalar spin order of parahydrogen among all spins in the low-field, strong-coupling network, is in quantitative agreement with the simulated spectra presented in Figure 3. The pattern of intensities is fully accounted for by the simulations. As seen in the inset of Figure 4, the H^2 and H^3 signals occur mostly with emission phase, but with unequal intensities.

The spectrum presented in Figure 4(d) was obtained upon lowering the reaction temperature to 200 °C. In comparison to the spectrum obtained at 350 °C, the ALTADENA signals of propane and propene have increased and decreased, respectively. This reveals that the selective hydrogenation of propyne to propene is favoured at higher temperatures, which is also the trend observed for palladium catalysts.[48] Figures 5(a) and (b) plot the integrated signal areas for the propane CH_3 and propene CH multiplets (visible in the stacked spectra shown in Figure S6 of the *ESI*) for a series of reaction temperatures between 200 and 375 °C for a 260/120/20 mL/min $N_2/H_2/C_3H_4$ reactant gas mixture (6:1 H_2:propyne) containing p-H_2 or n-H_2.

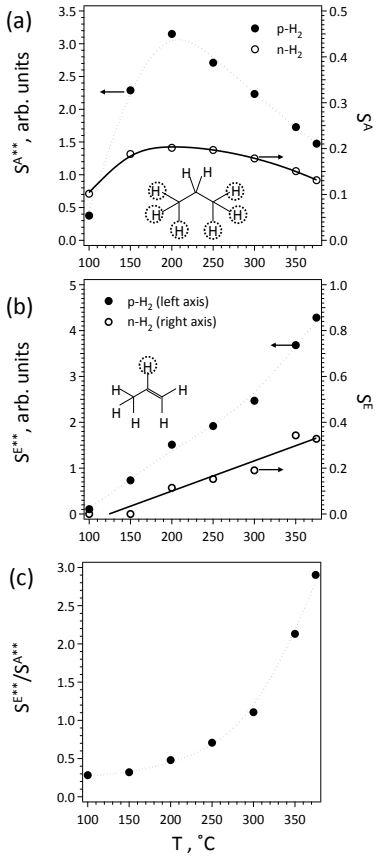

Figure 5. Reaction temperature dependence of the integrated proton NMR signals resulting from reactions with n-H_2 (open circles) and p-H_2 (filled circles) at a (6:1 H_2:propyne) reactant ratio (260/120/20 mL/min of $N_2/H_2/C_3H_4$, respectively). The arbitrary units are the same for all parts of this figure. (a) Peak integrals for ALTADENA (left axis) and thermally polarized (right axis) propane CH_3 group signals, S^{A**} and S^A, respectively. (b) ALTADENA (left axis) and thermally polarized (right axis) propene H^1 signals, S^{E**} and S^E, respectively. The ALTADENA integrals were measured from the difference spectra (see text). Thermally polarized signals were corrected for incomplete relaxation. ALTADENA signals were corrected for relaxation losses. The thermally polarized propane CH_3 signal has been divided by 6 to yield the signal contribution per proton. (c) Ratio of propene H^1 and propane CH_3 ALTADENA signals.

A lower H_2:propyne ratio was selected for this experiment to increase the selectivity to propene over propane compared with the 12:1 H_2:propyne ratio. Total propane formation, represented by the relaxation-corrected thermally polarized signals obtained using n-H_2, increases between 100 and 200 °C and then gradually declines between 200 and 375 °C. The propane ALTADENA signals recorded over the same temperature range and reaction mixture exhibit a similar trend. In contrast, Figure 5(b) shows that the thermally polarized and ALTADENA propene signals, representing total and pairwise conversion to propene, increase monotonically with temperature and exhibit a linear increase with temperature up to 300 °C. Consequently, the propene/propane ALTADENA NMR signal ratio S^{E**}/S^{A**} increases sharply with increasing temperature, as seen in Figure 5(c). These results show that partial reduction selectivity is maximal at high reaction temperature where desorption of propene effectively competes with hydrogenation to propane. This behaviour is observed for all H_2: propyne ratios investigated. For brevity only representative data for one H_2:propyne ratio is presented.

Figure 6 presents the propene CH_2 region of the ALTADENA spectra acquired using the 6:1 H_2:propyne reactant mixture (constant total flow rate of 400 mL/min) acquired over the 100-375 °C range. The experimental spectra (in blue) were fit to a linear combination of simulated *syn* and *anti* pairwise addition spectra (in black) taking the weighting coefficients as fitting parameters in eqn (1). Stereoselectivity, calculated by eqn (2), is plotted as a function of reaction temperature in Figure 6(b) for three p-H_2:substrate ratios (6:1, 12:1, and 18:1) at fixed propyne pressure and a fixed total flow rate of 400 mL/min. *Syn* addition stereoselectivity is found to be a monotonically increasing function of temperature.

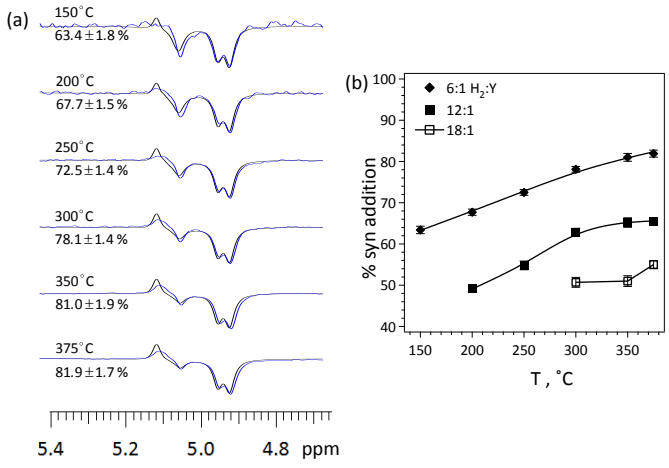

Figure 6. Least-squares fits of experimental ALTADENA difference spectra to a linear combination of simulated *syn* and *anti* addition ALTADENA (see eqn (1)) spectra allowing c_{syn} and c_{anti} to vary. (a) Fitting results (in black) are superimposed on the data (in blue) which were acquired using a 260/120/20 mL/min $N_2/H_2/C_3H_4$ reactant gas mixture (6:1 H_2:propyne, total flow rate of 400 mL/min, 1 bar) at the series of reaction temperatures indicated. (b) Temperature dependence of the pairwise *syn* addition stereoselectivity, defined in eqn (2), for three different H_2:propyne ratios.

Effect of Hydrogen Partial Pressure. Further reaction studies were performed at constant temperature while varying the n-H_2 or p-H_2 partial pressure from 0.15 to 0.95 bar, corresponding to H_2/propyne pressure ratios ranging from 3 to 19, while maintaining fixed propyne pressure ($P_Y = 0.05$ bar) and constant total flow rate (400 mL/min). A temperature of 350 °C was selected for these experiments to maximize the propene contribution. Stacked plots of the raw NMR spectra (without subtraction or baseline correction) acquired using 10 mg of catalyst are presented in Figure 7.

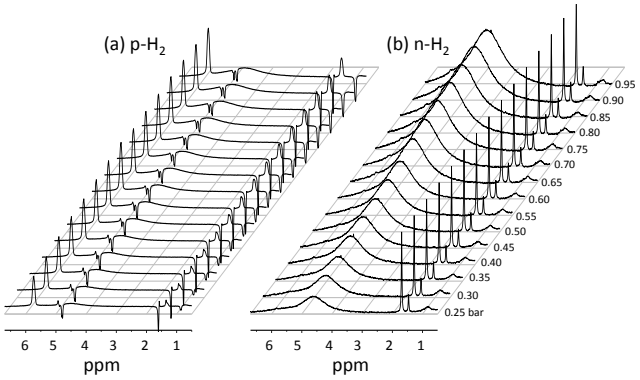

Figure 7. 400 MHz proton NMR spectra acquired for a series of (a) p-H_2 or (b) n-H_2 partial pressures using 10 mg of Pt/TiO_2 catalyst at a reactor temperature of 350 °C and constant total flow rate of 400 mL/min. The propyne pressure was held constant at 50 mbar. Raw spectra (not difference spectra) are presented in this figure. The broad peak centered near 4.7 ppm is due to o-H_2. The peak centered near ~1.6 ppm in (a) results from the superposition of thermally polarized (absorption phase) propyne and ALTADENA polarized (emission phase) propene methyl group signals, which have slightly different chemical shifts. The spectrum is correctly phased.

A second data set was acquired using a larger amount of catalyst (50 mg) to increase the thermally polarized signals (see Figures S7 and S8 of the *ESI*). As seen in Figure 7(a), the propene and propane ALTADENA signals intensify with increasing p-H_2 partial pressure, and qualitative changes in the propene CH_2 region are apparent. Even by inspection of the spectra it can be seen that the *syn* addition stereoselectivity decreases markedly with increasing p-H_2 partial pressure. In the data acquired using n-H_2 (Figure 7(b)), the broad peak due to o-H_2 and the sharp peaks between 1.5 and 2 ppm (due to propyne) dominate the spectrum, while the thermally polarized propene and propane peaks are barely seen above the noise. Figure 8(a) presents a summary plot of the propane signals obtained using 50 mg, which are significantly stronger than those obtained with 10 mg of catalyst. The thermally polarized propene and propane signals obtained using 10 mg of catalyst are too weak to report (see Figure 7(b)). An approximate linear increase in S^{A**} with p-H_2 partial pressure is observed with both catalyst amounts.

The propane and propene ALTADENA polarized signals obtained with 10 mg catalyst at 350 °C are presented in Figure 8(b) as a function of hydrogen partial pressure. Note that the propene signal S^{E**} plateaus at pressures where the propane signal S^{A**} continues to climb. The ratio S^{E**}/S^{A**} is plotted over the 0.25 to 0.95 bar p-H_2 pressure range for both catalyst amounts in Figure 8(c). The different signal ratios for the two

catalyst amounts reveal that that the S^{E**}/S^{A**} ratio is dependent on catalyst contact time. The more time that is spent near the catalyst (increasing amount of catalyst) the higher the likelihood of propene reacting to propane. Even though the S^{E**}/S^{A**} ratios differ by almost a factor of two, they exhibit a similar trend, and at 350 °C the signal ratio for each catalyst drops by a factor of about 3 over the same pressure range. A log plot of the same data is shown in Figure 8(d). The solid lines represent least squares fits of the linear region (high H_2 partial pressure). At 350 °C, the fitted slope is close to -1 for both catalyst amounts (*i.e.* well-within the experimental uncertainty), consistent with reaction orders of one and two for the single and double hydrogenation, respectively, and suggesting that the surface hydrogen density is proportional to H_2 partial pressure at this high reaction temperature. For the same pressure range at 200 °C, where the propane signals are substantially stronger than the propene signals, the ratio decreases from $S^{E**}/S^{A**} = 0.6$ to 0.2.

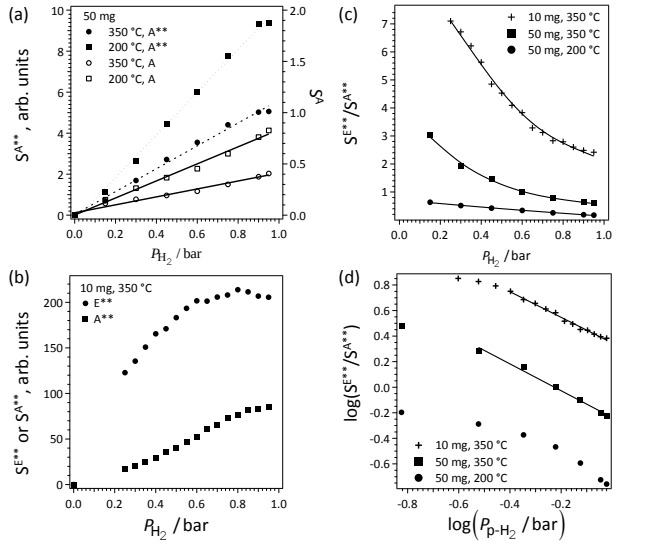

Figure 8. Dependence of the propane (A) and propene (E) signals on n-H_2 or p-H_2 partial pressure at a reaction temperature of 350 °C. (a) ALTADENA (left axis) and thermally polarized (right axis) propane CH_3 signal integrals acquired using 50 mg Pt/TiO_2 catalyst. (b) Propene ^{1}H and propane CH_3 ALTADENA signal integrals obtained at 350 °C using 10 mg catalyst. (c) Propene:propane ALTADENA signal ratios obtained with 10 mg and 50 mg catalyst. (d) Log plot of the same data presented in (c) together with linear least squares fits in the high H_2 pressure regime (see text) where the data exhibits a linear trend. Note that different arbitrary units are used in parts (a) and (b).

A plot of the propene CH_2 region of the ALTADENA spectra acquired as a function of p-H_2 pressure at 350 °C is presented in Figure 9(a). Best fit spectra (in blue) are superimposed on each of the experimental spectra (in black). The fitting results reveal that the pairwise *syn* stereoselective addition to propyne decreases from 90% to 52% over the $P_{p\text{-}H_2}$ = 0.15 bar (3:1 H_2:propyne) to 0.95 bar (19:1 H_2:propyne) range. The summary plot for this data set, Figure 9(b), reveals a linear decrease in *syn* addition stereoselectivity with increasing H_2 partial pressure and approaches 50% (non-stereoselective) at 0.95 bar. The data obtained using 10 mg of catalyst exhibited a similar dependence on $P_{p\text{-}H_2}$ (as seen in Figure 7a). The series of spectra obtained when the temperature was reduced to 200 °C (using 50 mg amount of catalyst) are shown in Figure S9. Although the spectral fitting analysis was not applied to this data set, the changes in the propene CH_2 region exhibit a similar decrease in the *syn* addition stereoselectivity when the p-H_2/propyne ratio is increased.

Reaction Mechanism. The trends in our data are readily interpreted with the aid of the scheme proposed in Figure 2. Firstly, our data suggest that pairwise addition to propyne is intrinsically stereoselective, with >90% yield in the *cis* disposition of bilinear spin order, under conditions that favour selective hydrogenation to propene. A reasonable assumption is that in a pairwise addition process, H-atoms in a spin-correlated pair will attack the triple bond from a common origin on one side or the other of the π-adsorbed propyne molecule, probably in a concerted process involving adsorbed molecular H_2. At high reaction temperatures (≥300 °C), propene desorption occurs at a relatively high rate and *cis*-propene is released into the gas phase before any subsequent surface transformations can occur. As the reaction temperature is reduced, the propene residence time increases and therefore the probability for half-hydrogenation or full reduction will also increase, as does the propensity for *cis-trans* isomerization. These trends are evident in Figures 5 and 6. Increasing the contact time (increasing amounts of catalyst) has a similar effect, as the longer the reaction species are in contact with the catalyst, the higher the probability for full reduction (Figure 8). Figure 8 also confirms the expectation that second reduction is favored by high H_2 partial pressure. Half hydrogenation to the 2-propyl form or hydrogenation to propane consumes surface hydrogen and therefore the rates of these processes are expected to be suppressed at low surface H densities. The second reduction can occur either by direct saturation or step-wise addition via the 2-propyl intermediate. This key surface species also mediates *cis-trans* isomerization, leaving the H^2 and H^3 positions randomized upon reversion to π-adsorbed propene, resulting in a loss of the apparent stereoselectivity in the desorbed propene.

Interestingly, the linear trend in the *syn* addition stereoselectivity plotted in Figure 9(b) approaches 50% at higher p-H_2 pressures, indicating non-stereoselective hydrogenation. This could be due to an increasing amount of the 2-propyl intermediate which mediates cis-trans isomerization or simply more surface hydrogen atoms which can attack the triple bond from either side. However, it should be noted that double bond migration, which has the effect of exchanging the chemical shifts of the CH_2 and CH_3 protons, is not considered in the calculations. The fraction of propene molecules that undergo *cis-trans* isomerization via the 2-propyl species should be accompanied by an equal fraction undergoing double bond migration. The density matrix simulation of the spectrum that would result from double bond migration immediately following pairwise addition to propyne has been discussed above and is presented in the top panel of Figure 3. Note that the H^3 multiplet in this simulated spectrum exhibits absorption phase, which is opposite to the phase obtained in the *cis* disposition in propene, but with relatively low intensity. Hence, the superposition of a spectral contribution from the

propene fraction which has undergone double bond migration isomerization would have the effect of lowering the apparent *syn* addition stereoselectivity obtained from the fits to eqn (1), which neglects this contribution.

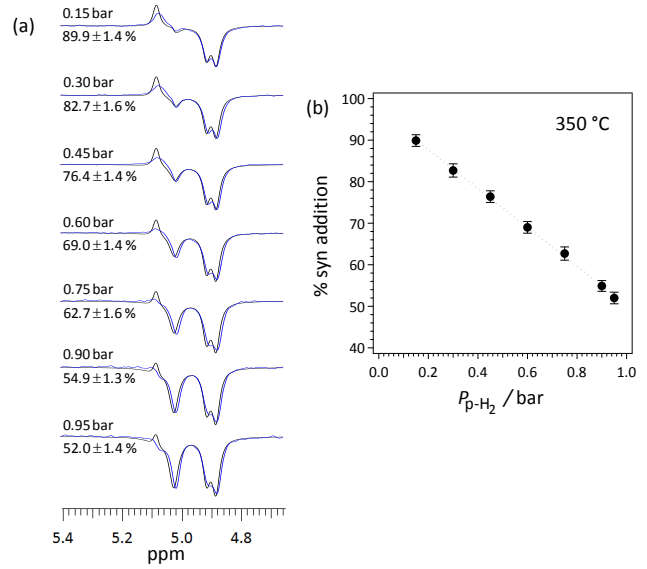

Figure 9. Results of least-squares spectral fitting of the propene CH_2 (H^2 and H^3) region of the experimental ALTADENA spectrum to a linear combination of simulated pairwise *syn* and *anti* addition spectra (eqn (1)). (b) Dependence of the *syn* addition stereoselectivity on hydrogen partial pressure over the $P_{p\text{-}H_2}$ = 0.15 to 0.95 bar range at 350 °C and a total flow rate of 400 mL as obtained from the least squares fits show in part (a) and eqn (2) using 50 mg of catalyst.

Conclusion

PHIP-NMR has proven to be a unique new tool for studying heterogeneous hydrogenation catalysis that can reveal previously hidden steps of surface reactions. Information about the stereoselectivity of pairwise addition to a triple bond and the subsequent randomization of the CH_2 protons by *cis-trans* isomerization is inaccessible by any other chemical method. Whilst analysis (by conventional NMR or mass spectrometry) of the products of reactions with D_2 or D_2/H_2 mixtures have been used in more recent years to investigate hydrogen exchange in transition metal complexes and metal nanoparticles,[28, 49] this approach does not provide unambiguous evidence for a pairwise addition path and cannot be used to trace pairs of nuclei through multiple reaction steps such as isomerization facilitated by the propyl intermediate, as we have done using ALTADENA/PHIP NMR.

Our results demonstrate that pairwise *syn* addition stereoselectivity is correlated to partial reduction selectivity. By systematically varying the reaction conditions, we found that low H_2:substrate ratio and high reaction temperature favours *syn* addition and high partial reduction selectivity. A *syn* pairwise addition stereoselectivity of 90% is obtained while simultaneously achieving a 7:1 propene:propane pairwise addition product ratio at 350 °C and 0.15 bar p-H_2. The trends in our experimental data have been rationalized in terms of the expected inverse relationship between propene/propane with H_2 partial pressure. Furthermore, the scheme presented in Figure 2 accounts for the observed correlation between *syn* addition stereoselectivity and propyne partial reduction selectivity in terms of established surface processes and surface species relevant to heterogeneous hydrogenation of olefins over Pt. The ability to use experimental conditions to control the disposition of the hyperpolarized bilinear spin order derived from parahydrogen following pairwise addition or replacement, together with partial reduction selectivity in substrates with triple bonds or multiple double bonds, could be important for the optimization of PHIP signals on substrates for specific applications.

Acknowledgements

The TEM work was carried out by Dr. Yan Xin at Florida State University, and the TEM facility at FSU is funded and supported by the Florida State University Research Foundation, National High Magnetic Field Laboratory (NSF-DMR-0654118) and the State of Florida. We thank M.H. Levitt for providing SpinDynamica ALTADENA simulation examples and helpful discussions. Postdoctoral support from the University of Florida through startup funds are gratefully acknowledged (Hagelin-Weaver).

Notes and references

1. C. R. Bowers and D. P. Weitekamp, *Phys. Rev. Lett.*, 1986, **57**, 2645-2648.
2. C. R. Bowers and D. P. Weitekamp, *J. Am. Chem. Soc.*, 1987, **109**, 5541-5542.
3. T. C. Eisenschmid, R. U. Kirss, P. P. Deutsch, S. I. Hommeltoft, R. Eisenberg, J. Bargon, R. G. Lawler and A. L. Balch, *J. Am. Chem. Soc.*, 1987, **109**, 8089-8091.
4. M. G. Pravica and D. P. Weitekamp, *Chem. Phys. Lett.*, 1988, **145**, 255-258.
5. R. Eisenberg, *Acc. Chem. Res.*, 1991, **24**, 110-116.
6. C. R. Bowers, in *Encyclopedia of Nuclear Magnetic Resonance*, eds. D. M. Grant and R. K. Harris, John Wiley & Sons, Ltd., Chichester, 2002, vol. 9, p. 750.
7. R. W. Adams, J. A. Aguilar, K. D. Atkinson, M. J. Cowley, P. I. P. Elliott, S. B. Duckett, G. G. R. Green, I. G. Khazal, J. Lopez-Serrano and D. C. Williamson, *Science*, 2009, **323**, 1708-1711.
8. L.-S. Bouchard, S. R. Burt, M. S. Anwar, K. V. Kovtunov, I. V. Koptyug and A. Pines, *Science*, 2008, **319**, 442-445.
9. K. V. Kovtunov, V. V. Zhivonitko, A. Corma and I. V. Koptyug, *J. Phys. Chem. Lett.*, 2010, **1**, 1705-1708.
10. I. V. Skovpin, V. V. Zhivonitko, R. Kaptein and I. V. Koptyug, *Appl Magn Reson*, 2013, **44**, 289-300.
11. K. V. Kovtunov, V. V. Zhivonitko, I. V. Skovpin, D. A. Barskiy, O. G. Salnikov and I. V. Koptyug, *J. Phys. Chem. C*, 2013, **117**, 22887-22893.
12. F. Shi, A. M. Coffey, K. W. Waddell, E. Y. Chekmenev and B. M. Goodson *Angew. Chem. Int. Ed.*, 2014, **53**, 7495-7498.
13. S. Glöggler, A. M. Grunfeld, Y. N. Ertas, J. McCormick, S. Wagner, P. P. M. Schleker and L.-S. Bouchard, *Angewandte Chemie International Edition*, 2015, **54**, 2452-2456.
14. R. H. Zhou, E. W. Zhao, W. Cheng, L. M. Neal, H. B. Zheng, R. E. Quinones, H. E. Hagelin-Weaver and C. R. Bowers, *J. Am. Chem. Soc.*, 2015, **137**, 1938-1946.

15. N. Eshuis, N. Hermkens, B. J. A. van Weerdenburg, M. C. Feiters, F. P. J. T. Rutjes, S. S. Wijmenga and M. Tessari, *J. Am. Chem. Soc.*, 2014, **136**, 2695-2698.
16. B. J. A. van Weerdenburg, S. Gloggler, N. Eshuis, A. H. J. Engwerda, J. M. M. Smits, R. de Gelder, S. Appelt, S. S. Wymenga, M. Tessari, M. C. Feiters, B. Blumich and F. P. J. T. Rutjes, *Chem. Commun. (Cambridge, U. K.)*, 2013, **49**, 7388-7390.
17. I. V. Koptyug, K. V. Kovtunov, S. R. Burt, M. S. Anwar, C. Hilty, S.-I. Han, A. Pines and R. Z. Sagdeev, *J. Am. Chem. Soc.*, 2007, **129**, 5580-5586.
18. K. V. Kovtunov, I. E. Beck, V. I. Bukhtiyarov and I. V. Koptyug, *Angew. Chem. Int. Ed.*, 2008, **47**, 1492-1495.
19. V. V. Zhivonitko, K. V. Kovtunov, I. E. Beck, A. B. Ayupov, V. I. Bukhtiyarov and I. V. Koptyug, *J. Phys. Chem. C*, 2011, **115**, 13386-13391.
20. O. G. Salnikov, K. V. Kovtunov, D. A. Barskiy, V. I. Bukhtiyarov, R. Kaptein and I. V. Koptyug, *Appl Magn Reson*, 2013, **44**, 279-288.
21. K. V. Kovtunov, V. V. Zhivonitko, I. V. Skovpin, D. A. Barskiy and I. V. Koptyug, *Top Curr Chem*, 2013, **338**, 123-180.
22. A. Corma, O. G. Salnikov, D. A. Barskiy, K. V. Kovtunov and I. V. Koptyug, *Chem.--Eur. J.*, 2015, **21**, 7012-7015.
23. D. A. Barskiy, O. G. Salnikov, K. V. Kovtunov and I. V. Koptyug, *The Journal of Physical Chemistry A*, 2015, **119**, 996-1006.
24. S. B. Duckett and C. J. Sleigh, *Prog. Nucl. Magn. Reson. Spectrosc.*, 1999, **34**, 71-92.
25. S. K. Hasnip, S. B. Duckett, C. J. Sleigh, D. R. Taylor, G. K. Barlow and M. J. Taylor, *Chem. Commun. (Cambridge, U. K.)*, 1999, 1717-1718.
26. D. Blazina, S. B. Duckett, J. P. Dunne and C. Godard, *Dalton Trans.*, 2004, 2601-2609.
27. J. P. Dunne, D. Blazina, S. Aiken, H. A. Carteret, S. B. Duckett, J. A. Jones, R. Poli and A. C. Whitwood, *Dalton Trans.*, 2004, 3616-3628.
28. J. Matthes, T. Pery, S. Grundemann, G. Buntkowsky, S. Sabo-Etienne, B. Chaudret and H. H. Limbach, *J. Am. Chem. Soc.*, 2004, **126**, 8366-8367.
29. M. Boutain, S. B. Duckett, J. P. Dunne, C. Godard, J. M. Hernandez, A. J. Holmes, I. G. Khazal and J. Lopez-Serrano, *Dalton Trans.*, 2010, **39**, 3495-3500.
30. K. V. Kovtunov, I. E. Beck, V. V. Zhivonitko, D. A. Barskiy, V. I. Bukhtiyarov and I. V. Koptyug, *Phys Chem Chem Phys*, 2012, **14**, 11008-11014.
31. I. Horiuti and M. Polanyi, *T Faraday Soc*, 1934, **30**, 1164-1172.
32. G. C. Bond, *Metal-catalysed reactions of hydrocarbons*, Springer Science, New York, 2005.
33. G. C. Bond and P. B. Wells, *Adv Catal*, 1964, **15**, 91-226.
34. B. Yang, X. Q. Gong, H. F. Wang, X. M. Cao, J. J. Rooney and P. Hu, *J. Am. Chem. Soc.*, 2013, **135**, 15244-15250.
35. G. Vile, D. Baudouin, I. N. Remediakis, C. Coperet, N. Lopez and J. Perez-Ramirez, *Chemcatchem*, 2013, **5**, 3750-3759.
36. S. J. Pennycook and L. A. Boatner, *Nature*, 1988, **336**, 565-567.
37. Rasband, W.S., ImageJ, U. S. National Institutes of Health, Bethesda, Maryland, USA, http://imagej.nih.gov/ij/, 1997-2014.
38. D. C. Bregel, S. M. Oldham and R. Eisenberg, *J. Am. Chem. Soc.*, 2002, **124**, 13827-13832.
39. G. C. Bond, Phillips.Jj, J. M. Winterbottom and P. B. Wells, *T Faraday Soc*, 1964, **60**, 1847-1864.
40. B. Mattson, W. Foster, J. Greimann, T. Hoette, N. Le, A. Mirich, S. Wankum, A. Cabri, C. Reichenbacher and E. Schwanke, *J. Chem. Educ.*, 2013, **90**, 613-619.
41. G. C. Bond, *Annu. Rep. Prog. Chem., Set. A. Gen. Phys and Inorg. Chem.*, 1968, **65**, 121-128.
42. G. C. Bond, *Heterogeneous catalysis : principles and applications*, Clarendon Press, Oxford Oxfordshire ; New York, 2nd edn., 1987.
43. G. J. Kubas, *Acc. Chem. Res.*, 1988, **21**, 120-128.
44. D. A. Barskiy, K. V. Kovtunov, A. Primo, A. Corma, R. Kaptein and I. V. Koptyug, *Chemcatchem*, 2012, **4**, 2031-2035.
45. N. N. Jarenwattananon, S. Gloggler, T. Otto, A. Melkonian, W. Mlorris, S. R. Burt, O. M. Yaghi and L. S. Bouchard, *Nature*, 2013, **502**, 537-541.
46. M. H. Levitt, J. Rantaharju, A. Brinkmann and www.SpinDynamica.soton.ac.uk.
47. K. L. Ivanov, A. N. Pravdivtsev, A. V. Yurkovskaya, H. M. Vieth and R. Kaptein, *Prog. Nucl. Magn. Reson. Spectrosc.*, 2014, **81**, 1-36.
48. H. Bazzazzadegan, M. Kazemeini and A. M. Rashidi, *Appl Catal a-Gen*, 2011, **399**, 184-190.
49. J. García-Antón, M. R. Axet, S. Jansat, K. Philippot, B. Chaudret, T. Pery, G. Buntkowsky and H.-H. Limbach, *Angewandte Chemie International Edition*, 2008, **47**, 2074-2078.

Table of Contents Image

The surface processes resulting in the anticorrelation of semi-hydrogenation selectivity and stereoselective addition to propyne are revealed by parahydrogen enhanced NMR.